American Mineralogist, Volume 84, pages 1213–1223, 1999

Variability of apatite fission-track annealing kinetics: I. Experimental results

WILLIAM D. CARLSON,[1] RAYMOND A. DONELICK,[2,*] AND RICHARD A. KETCHAM[1,†]

[1]Department of Geological Sciences, University of Texas at Austin, Austin, Texas 78712, U.S.A.
[2]Department of Geology and Geophysics, Rice University, Houston, Texas 77005, U.S.A.

ABSTRACT

Annealing rates for fission tracks in apatite vary markedly as a complex function of composition, based on an experimental study of 15 well-characterized, compositionally diverse apatites. Extensive annealing data were obtained in 69 experiments (durations of 1, 10, 100, and 1000 h at temperatures from 75 to 400 °C) on each of four apatites, three with near end-member occupancy of the halogen site by F, Cl, and OH, plus the well-known apatite from Durango, Mexico. These results were supplemented by less-comprehensive annealing data from 12 experiments over the same range of time and temperature on each of the remaining 11 apatites. Measurements of initial fission-track length, a parameter of considerable importance to the derivation of time-temperature paths from fission-track data, reveal substantial variations from one apatite to another; initial lengths are best predicted from etch figures. Interlaboratory comparisons of data on annealing kinetics highlight discrepancies that appear to result largely from differences in the precision and accuracy of experimental temperatures. None of the factors previously proposed as the dominant compositional controls on annealing rates can account completely for annealing behavior over the full range of compositions studied. Nevertheless, relative rates of annealing among all apatites are highly systematic, which allows this data set to be used in its entirety to constrain multikinetic annealing models that predict fission-track lengths as a function of time and temperature.

INTRODUCTION

Rates of thermal annealing of fission tracks in apatite depend strongly upon the chemical composition of the host crystal. Dramatic evidence of the effect of composition on track retention is seen, for example, in the disparate fission-track ages reported by Green et al. (1986, their Fig. 13) for multiple apatite crystals from a single deeply buried borehole sample, a sandstone of the Otway Group whose sediments were derived from contemporaneous volcanism. In this sample, individual grain ages range from zero to the depositional age of the rock itself (~120 Ma), and correlate with Cl content of the apatite crystals. If neglected, this sensitivity of annealing rates to apatite chemistry may severely limit the precision of thermal histories derived from partially annealed fission-track populations in apatite crystals with a range of composition, because models for thermal annealing calibrated by experiments on a single apatite will not accurately predict the annealing behavior of fission tracks in a compositionally diverse population. Conversely, if the variation in annealing behavior for apatites of different composition could be quantified, the range of temperature over which apatite fission tracks serve as recorders of thermal history could be extended and the precision of thermal histories could be improved; more-resistant apatites could be used to probe the higher-temperature portions of a rock's history, whereas less-resistant apatites could be used to monitor the lower-temperature portions.

In this article, we present experimental data on the rates of fission-track annealing in 15 well-characterized apatites of widely diverse chemistry, and compare our results to previously published experimental work. Companion articles present a technique for increasing the precision of analyses of natural and experimental fission-track measurements by accounting for the dependence of annealing rate on crystallographic orientation (Donelick et al. 1999, this volume), and introduce (Ketcham et al. 1999, this volume) a multikinetic empirical model, based on these new experimental data, that can be used to predict the thermal annealing behavior of apatite in compositionally diverse populations as a function of time and temperature.

EXPERIMENTAL METHODS

The apatite specimens in this work, chosen for both practical and theoretical utility, were characterized chemically and structurally, then pre-heated to eradicate natural tracks, irradiated to induce new tracks, subjected to isothermal annealing at carefully controlled temperatures for fixed periods of time, and etched to reveal tracks for measurement. Details of sample selection, characterization, and experimental methods are given below.

Sample selection

Specimens chosen for this study included (1) several different compositions representative of the range likely to be encountered in natural applications of thermal history analysis; (2) for comparative purposes, the Durango apatite used in experiments by Green et al. (1986) and Duddy et al. (1988), the Tioga apatite used in experiments by Donelick et al. (1990) and Donelick (1991), and apatites similar in composition but

*Current address: Department of Geology and Geological Engineering, University of Idaho, Moscow, Idaho 83844, U.S.A.
†E-mail: richk@maestro.geo.utexas.edu

TABLE 1. Characteristics of apatite specimens

Apatite symbol	Locality	Source	Source information	Material analyzed	Distinctive chemistry	Conditions of total annealing	Minutes near core	Age of run 0 fission tracks (d)
AY	Ayacucho, Peru	obtained commercially		1 mm slabs cut parallel to *c* axis	Cl = 0.24	17 h, 30 min 500 °C	197	416
B2	Bamble, Norway	Smithsonian Institution	NMNH B-13064	randomly oriented chips ≤300 μm	Cl = 0.87 OH = 0.98	167 h, 10 min 450 °C	197	416
B3	Bamble, Norway	Smithsonian Institution	NMNH 114937	randomly oriented chips ≤300 μm	Cl = 1.87	167 h, 10 min 450 °C	197	416
DR	Cerro de Mercado, Durango, Mexico	University of Texas at Austin	Barron Collection	1 mm slabs cut parallel to *c* axis	Cl = 0.12	170 h, 10 min 425 °C	133	416
FC	Fish Canyon Tuff, San Juan Mtns., Colorado, U.S.A.	Donelick Analytical, Inc.		euhedral crystals ≤300 μm	Cl = 0.24 OH = 0.63	167 h, 10 min 450 °C	86	420
HS	Holly Springs, Georgia, U.S.A.	Smithsonian Institution	NMNH R9498	randomly oriented chips ≤300 μm	OH = 1.83 Cl = 0.10	167 h, 10 min 450 °C	197	416
KP	Kola Peninsula, Russia	Smithsonian Institution	NMNH 136827	randomly oriented chips ≤300 μm	SrO = 0.94 Na_2O = 0.26	167 h, 10 min 450 °C	197	416
OL	Otter Lake, Quebec, Canada	obtained commercially		1 mm slabs cut parallel to *c* axis	F = 1.74	167 h, 10 min 450 °C	12	415
PC	Portland, Connecticut, U.S.A.	Harvard Mineral Museum	20434	1 mm slabs cut parallel to *c* axis	MnO = 1.02	21 h, 0 min 500 °C	7	521
PQ	Panasqueira, Portugal	Smithsonian Institution	NMNH 145294	1 mm slabs cut parallel to *c* axis		167 h, 10 min 450 °C	102	416
RN	Renfrew, Rensselaer Ontario, Canada	Polytechnic Institute	Don Miller personal collection	1 mm slabs cut parallel to *c* axis		18 h, 0 min 530 °C	55	420
SC	Silver Crater, Ontario, Canada	Rensselaer Polytechnic Institute	Mary Roden-Tice personal collection	1 mm slabs cut parallel to *c* axis		18 h, 0 min 530 °C	55	420
TI	Tioga ash bed near Old Port, Pennsylvania, U.S.A.	Rensselaer Polytechnic Institute		euhedral crystals ≤300 μm	Cl = 0.17 OH = 0.94 Fe = 0.12	12 h, 0 min 500 °C	55	420
UN	unknown	Dalhousie University	student mineralogy collection	1 mm slabs cut parallel to *c* axis	OH = 0.47	170 h, 10 min 425 °C	197	416
WK	Wakefield, Ontario, Canada	Rensselaer Polytechnic Institute	Don Miller personal collection	1 mm slabs cut parallel to *c* axis		18 h, 0 min 530 °C	197	416

Note: Compositional information is number of apfu, based on end-member composition of $Ca_{10}(PO_4)_6F_2$.

not identical to those used in experiments by Crowley et al. (1991); (3) several extreme compositional variants, not likely to be encountered in natural applications, but potentially able to yield information on the underlying principles governing compositional effects on annealing behavior; and (4) several near-end-member Ca-F apatites useful for exploring the range of variation in annealing behavior that might be attributable to factors other than composition. We sought specimens with the greatest available degree of compositional homogeneity. Table 1 lists the locality, source, key chemical features, and irradiation parameters for each specimen.

The apatites were obtained in the form of either euhedral megacrysts, fragments of megacrysts, or a collection of small euhedral crystals. Megacrysts with a well-developed prismatic crystal face were cut into 1 mm thick slabs parallel to their crystallographic *c*-axes using a diamond wafering saw. Fragments of megacrysts were crushed using a mortar and pestle, then sieved to obtain randomly oriented fragments of <300 μm maximum diameter. Collections of euhedral grains with maximum diameters <300 μm were obtained from bulk rock samples using standard gravimetric and magnetic mineral separation methods.

Compositions

For specimens used in annealing experiments, electron probe microanalysis for major elements and selected trace elements was performed using wavelength-dispersive methods on a JEOL 733 Superprobe at the University of Texas at Austin. For all elements, well-characterized natural and synthetic minerals and glasses were used as standards. Except for measurements of Ce and La, analyses were made with an accelerating voltage of 15 kV, a beam current of 15 nA on brass, a beam diameter of 10 μm, and counting times of 30 s; data reduction employed the correction factors of Albee and Ray (1970). Ce and La were analyzed in separate runs at 15 kV and 30 nA with a beam diameter of 30 μm for 120 s; a ZAF correction was used for data reduction. Analysis of F was aided by the high count rates generated by an interlayered W-Si pseudocrystal used for wavelength dispersion in the detector. Nevertheless, these analyses were problematic because count rates for F in apatite vary with time as a function of crystallographic orientation, in response to diffusion driven by electron implantation (cf. Stormer et al. 1993). To minimize these effects for megacrystic specimens, sections of unknown and standard crystals oriented parallel to

the *c* crystallographic axis were prepared, on which the time variation of count rates was small and similar for both standards and unknowns. For polygranular samples, count rates were monitored on randomly oriented sections, and analyses were made on those grains for which the temporal variation was smallest. Hydroxyl contents were determined by difference, assuming full occupancy of the halogen site by F, Cl, and OH. On megacrystic specimens, analyses were made at 6–18 points ranging from core to rim of the crystal; on polygranular specimens, analyses were made of 20–30 randomly selected grains.

Unit-cell parameters

Crystal symmetry and unit-cell parameters were determined by powder X-ray diffractometry (XRD) on an automated Rigaku DMAX-II instrument with a graphite monochromator, using Cu*K*α radiation at 35 kV and 20 mA, scanning the 2θ region from 6° to 70° at 3°/min. An internal MgO standard allowed peak positions to be determined with a reproducibility in replicate runs ranging between ±0.05° (high-intensity peaks) and ±0.10° (low-intensity peaks). Cell parameters and their associated uncertainties were derived from measured peak positions using the least-squares fitting procedure of Novak and Colville (1989). Two separate XRD samples were prepared for each specimen, and duplicate diffraction spectra and fits were obtained.

Annealing experiments

Pre-treatment and irradiation. To remove naturally occurring fission tracks already present in the apatite crystals, the specimens were annealed at 1 atm in air at temperatures from 425 to 530 °C for times ranging from 12 to 170 h, then cooled slowly to room temperature. Irradiation to induce fission tracks was performed in site A-2 of the research reactor at the Nuclear Science Center, Texas A&M University, with the apatites in proximity to the reactor core for periods of time ranging from 7 to 197 min. The ambient temperature in the A-2 site is believed to be <50 °C (Bill Asher, personal communication, 1991).

Annealing. In these experiments, special attention was given to the need for accurate, precise, and reproducible annealing temperatures. Small amounts of each apatite were wrapped in aluminum foil, then bound together side-by-side in a packet no larger than 0.5–1 cm in maximum dimension. These sample packets were annealed in one of six vertical furnaces, each 32 cm long with an internal bore of either 2.5 or 3.2 cm. Each furnace used anti-convection endplugs and special furnace windings, more closely spaced at the ends than in the center, to minimize axial thermal gradients and thereby to create a large central isothermal zone, in which temperature varied by less than ±1 °C over axial distances of 3–5 cm. Sample packets were placed in the center of an isothermal zone, and located within 1 mm of the tip of a Pt/Pt_{90}-Rh_{10} thermocouple (matched pair, special grade). Output from the thermocouple was fed through Cu/Alloy 11 extension wires to an electronic cold-junction compensator (Omega Engineering MCJ/R-S) and into a microvoltmeter (Fluke Model 8840A). Voltages were converted to temperatures using a tabulation of the IPTS-68 scale (NIST Monograph 125; ninth-order polynomial). At the beginning and the end of the experiments, the microvoltmeter was calibrated against the output of a DC microvoltage calibrator (Fluke Model 343A), which had itself been factory-calibrated and certified against NIST-traceable temperature standards only a few days before; no detectable instrumental drift occurred over the course of the experimental program. The accuracy of these temperature measurements is ±1–2 °C, with nearly all of the uncertainty arising from the ±1 °C accuracy specified for the electronic cold-junction compensator. Performance of that compensator was checked by substituting a second identical device in its place; differences in the output voltage were negligible, corresponding to a small fraction of a degree.

The precision of annealing temperatures was governed principally by the ability of the temperature controllers regulating furnace power to maintain constant temperatures over time. Each furnace was connected to a three-term (PID) controller, adjusted to provide optimal damping of fluctuations at a temperature of 250 °C, approximately the center of the range of annealing temperatures used in this study. Temperatures were monitored periodically during all runs and, with few exceptions, temperature excursions were no greater than ±1 °C. (In one experiment, however, we believe a significant temperature error appears, perhaps because of mispositioning of the sample within the furnace. That experiment, run 49, was a quadruplicate run, for which the other three runs at nominally identical conditions yielded substantially more annealing. Results from run 49 were excluded from analysis.) Runs were quenched by simply withdrawing the sample from the furnace; cooling to room temperature required <1 min.

Another factor affecting the precision of reported annealing conditions is the time required for the sample assembly to reach thermal equilibrium after insertion into the furnace. Although the thermocouple reading was typically within 2 °C of its final value within 2–4 min after insertion, this equilibration time on run-up introduces a small ambiguity into the time-temperature path for short (1 h) runs. In these cases, we quenched the run one hour after the sample achieved a temperature within 2 °C of the nominal run temperature. At longer run times, thermal equilibration periods are an insignificant fraction of the total time-temperature history.

To provide realistic estimates of the overall uncertainties that should be attached to experimental determinations of fission-track annealing rates, our experimental design included numerous replicate runs with nominally identical temperatures and durations, but carried out separately, using different experimental charges heated in different furnaces and measured with different thermocouples.

Fission-track revelation and measurement. After annealing, apatite crystals were mounted in epoxy, polished, and etched for 20 s in a 5.5 *M* HNO_3 solution at 21 °C. Aliquants of the apatites were set aside for use in determining initial fission-track lengths; these were allowed to remain at ambient laboratory temperatures (believed not to have exceeded 23 °C) for times ranging from 415 to 521 days before measurement. During mounting, the epoxide resin was permitted to cure at ambient laboratory temperature. Once cured, the grain mounts were polished to expose internal surfaces of the apatite slabs,

fragments, or grains, using 0.3 μm alumina while taking care to avoid excessive frictional heating.

Measurements were made only on horizontal, confined, TINT fission tracks (TINT = Track-IN-Track, meaning confined tracks etched via a fission track emanating from the polished and etched apatite surface) lying in crystallographic planes parallel to the long axis of the fission-track etch figures (parallel to the crystallographic *c* axis in hexagonal apatites). All measurements were performed by a single investigator (RAD) using a single analytical system. In each experiment, the lengths and orientations of tracks were measured in transmitted light at 1563× magnification (12.5× oculars, 1.25× projection tube, 100× dry objective) using an automated stage and a calibrated digitizing pad with a projected LED cursor interfaced to a desktop computer, in a manner similar to that described in Donelick (1991). Repeated measurements performed on individual fission tracks indicate that the measurement precisions (1 standard deviation) of individual track lengths and track angles to the crystallographic *c* axis are approximately ±0.15 μm and ±2°, respectively. Specimens were encoded before track measurement, so that the investigator making the measurements was unaware of the temperature and duration of the annealing experiment, to avert any possible observer bias.

Heavily annealed samples in which only very small numbers of etched tracks were visible after initial examination were repolished, irradiated by proximity to a radioactive ^{252}Cf source to produce a standard areal density of ^{252}Cf tracks of $\sim 5 \times 10^6$ tracks/cm^2, then re-etched. This procedure increases the number of measurable tracks in populations with short mean lengths, but it also modifies the observational bias inherent in conventional track-revelation procedures, altering mean lengths by rendering visible a higher proportion of harder-to-detect tracks. As a result, the mean lengths measured in this way are discrepant in comparison with the rest of the data set, and were excluded from those parts of the later modeling and analysis that are based on mean lengths. However, when using *c*-axis projected lengths to correct measurements to a single reference orientation (cf. Donelick et al. 1999, this volume), the shift in length bias is removed, allowing these runs to be incorporated into models and analysis based on *c*-axis projected lengths. To understand better these biasing effects, some experiments were measured both with and without Cf-irradiation.

Etch figure measurement. D_{par}, the arithmetic mean maximum diameter of fission-track etch figures (Burtner et al. 1994; Donelick 1993, 1995), was determined for each apatite specimen with the same analytical system used to measure the fission-track lengths. Fission-track etch figures are the cross-section of the fission-track etch pits at the etched apatite surface (Honess 1927). For apatites etched as described above, fission-track etch figures are parallel to one another on prismatic surfaces of hexagonal apatites and their maximum diameters are aligned parallel to the crystallographic *c* axis. A minimum of 25 fission-track etch figures were measured for each apatite using reflected light. Although more precise results could be obtained using a scanning electron microscope, the decision was made to observe and measure etch-figure diameters using the optical microscope to provide a calibration that is more practicable and inexpensive to apply to the study of natural fission tracks.

RESULTS

Appendix Table 1, which is on deposit along with Appendix Tables 2 and 3 explained below, reports apatite compositions.[1] Each value listed is the average of 6–30 analyses; the uncertainties listed are standard errors of the mean, and indicate the degree of homogeneity within each specimen. To validate these compositional measurements, independent microprobe analyses on separate grain mounts were performed by the ARCO Exploration and Production Technology laboratory in Plano, Texas. Except for F and P, agreement between the two data sets was generally excellent, with few discrepancies that exceeded the range of uncertainty specified in Appendix Table 1. Discrepancies for F were common, however. These differences are reasonably explained by the fact that the ARCO analyses, like our initial analyses, were performed on unoriented mounts. As a result, all F analyses showed large variations and in some cases exceeded stoichiometric limits (cf. Stormer et al. 1993). These problems led us to repeat our F analyses on oriented specimens using the methods described in the section above on experimental methods; the tabulated values are those obtained from oriented specimens. Small systematic differences appeared between the two data sets for P, with the UT analyses consistently higher than the ARCO analyses by ~2% relative. Because some of our analyses yield very slight stoichiometric excesses for P, it is likely that our values for P are systematically high by this small amount. The cause of this error is unknown, but it may be the result of an inaccurate value for P in our standard, which is a crystal of Durango apatite, nominally 41.17 wt% P_2O_5, based on the average of gravimetric (41.09 wt%) and colorimetric (41.25 wt%) analyses performed by G.K. Hoops (University of Texas at Austin, 1974). The only other discrepancies that were larger than the cited uncertainties are in the Ce and Si contents of specimens PQ and OL. Because the concentrations of these elements vary antithetically with likely substituents (this is especially clear for Si and P), we believe the measured differences are real, and probably reflect intercrystalline inhomogeneity for these elements somewhat beyond the level indicated by the uncertainties given in Appendix Table 1.

The results of XRD determinations of crystal symmetry, cell parameters, and total ionic porosity (*Z*) are also given in Appendix Table 1. Differences between duplicate XRD runs were negligible, so the cited uncertainties in cell parameters are those produced by the calculations of Novak and Colville (1989). Although it is possible to index the XRD pattern of apatite B3 on an hexagonal cell (cf. JCPDS entry 24-214), and although single-crystal diffraction data is typically required to confirm the monoclinic symmetry of pseudo-hexagonal chlorapatites, we infer that B3 possesses monoclinic symmetry for two reasons. First, its XRD pattern is markedly different from those of all other specimens; it corresponds closely to the pattern of

[1]For a copy of Appendix Tables 1–3, document item AM-99-023, contact the Business Office of the Mineralogical Society of America (see inside front cover of recent issue) for price information. Deposit items may also be available on the American Mineralogist web site (http://www.minsocam.org or current web address).

natural monoclinic chlorapatite reported by Hounslow and Chao (1970) (JCPDS entry 24-214), but matches poorly the pattern of synthetic hexagonal chlorapatite (JCPDS replacement entry 27-74). Second, its Cl content of 1.87 Cl atoms per formula unit (apfu) just slightly exceeds the amount (1.82 Cl apfu) present in the monoclinic chlorapatite described by Hounslow and Chao (1970); these authors suggest that a transition to monoclinic symmetry is required when the Cl content exceeds some maximum value in the range 1.64–1.82 Cl apfu. Additional factors, including order/disorder on the halogen site, also have importance, however (cf. Hughes et al. 1989). Values of total ionic porosity were computed as in Carlson (1990, Eqs. 14 and Table 3). The final entries in Apppendix Table 1 are diameters of surface etch pits, measured in the direction parallel to the crystallographic *c* axis.

Appendix Tables 2a through 2d present annealing data for the four specimens on which we performed annealing experiments over the widest range of times and temperatures: runs were made at 25 °C intervals from 75 to 400 °C, for run durations of 1, 10, 100, and 1000 h. In addition to the previously studied Durango apatite, this more complete data set includes three specimens that closely approach end-member occupancy of the halogen site by F, Cl, and OH, with minimal substitution on cation sites. To complement data on mean fission-track length (l_m), we also report the mean length parallel and perpendicular to the crystallographic *c* axis (l_c and l_a, respectively). These values were calculated using the ellipse-fitting method described in Donelick (1991) except that, as described in Donelick et al. (1999, this volume) track populations that showed evidence of accelerated annealing at relatively high angles to the crystallographic *c* axis were excluded. Also tabulated are the modeled *c*-axis parallel values for each experiment ($l_{c,mod}$), which were calculated using the empirical formulation developed in Donelick et al. (1999, this volume).

Appendix Tables 3a through 3k present annealing data for the remaining apatite specimens. The set of experimental conditions for these specimens is less comprehensive than for the others, but annealing data are presented for each specimen along a 100 hour isochron and at conditions matching the limits of the more comprehensive data sets at low and high temperatures and for long and short durations.

DISCUSSION

Agreement among replicate experiments

Table 2 illustrates the level of agreement among mean track lengths measured on replicate experiments. With few exceptions, differences between nominally identical experiments are somewhat greater than the uncertainty arising from the error of individual measurements and are often greater than the dispersion of measured track lengths within a single experiment, even though great care has been taken to achieve precise and reproducible annealing temperatures. These differences tend to be greater in more thoroughly annealed samples, for which temperature variations of a few degrees can produce marked acceleration or deceleration of annealing. Even greater variations among replicate runs would be expected for experimental studies in which less precise temperature regulation was achieved. This fact has significance when making comparisons among annealing models based upon goodness-of-fit to the experimen-

TABLE 2. Mean track lengths (micrometers) in replicate experiments

t (h)	*T* (°C)	Run	RN	B3	HS	DR
1	150	62	16.05 (08)	16.53 (08)	16.45 (08)	15.94 (08)
		64	15.86 (08)	16.56 (08)	15.99 (09)	15.99 (07)
	175	10	15.80 (08)	16.38 (09)	15.43 (10)	15.72 (07)
		43	15.54 (08)	16.29 (08)	15.62 (08)	15.71 (07)
	250	5	14.36 (08)	15.66 (08)	14.56 (08)	14.94 (07)
		34	14.61 (06)	15.52 (08)	14.62 (06)	15.00 (08)
		35	14.83 (07)	15.49 (07)	14.82 (08)	15.23 (07)
	350	22	0.00	12.13 (11)	0.00	8.14 (26)
		63	0.00	11.82 (09)	0.00	10.03 (15)
10	200	2	15.36 (07)	15.92 (08)	14.99 (08)	15.12 (08)
		65	15.32 (07)	16.07 (08)	15.22 (08)	15.28 (08)
	250	1	13.80 (07)	14.77 (08)	13.17 (08)	14.07 (06)
		36	13.99 (08)	14.93 (08)	13.41 (07)	14.29 (07)
		37	14.12 (07)	14.93 (07)	13.75 (08)	14.35 (07)
100	75	55	16.05 (09)	16.73 (09)	16.39 (09)	15.99 (09)
		58	15.94 (08)	16.61 (07)	16.65 (09)	16.03 (07)
	125	27	15.68 (07)	16.30 (08)	15.93 (08)	15.84 (07)
		68	15.70 (08)	16.31 (09)	15.95 (08)	15.76 (07)
	175	14	15.17 (08)	15.85 (09)	15.08 (08)	15.28 (07)
		69	15.29 (07)	15.76 (08)	15.20 (08)	15.36 (07)
	225	13	13.81 (07)	14.80 (09)	13.44 (08)	14.44 (06)
		70	13.91 (08)	14.88 (09)	13.65 (08)	14.30 (07)
	250	6	12.24 (08)	13.95 (08)	11.36 (11)	13.59 (08)
		8	12.14 (08)	13.94 (08)	11.42 (11)	13.08 (09)
		15	12.11 (09)	14.28 (10)	11.76 (10)	13.01 (08)
		50	12.30 (08)	14.00 (09)	11.34 (09)	13.40 (07)
	275	16	8.71 (26)	13.02 (10)	9.12 (19)	11.12 (10)
		71	9.41 (15)	13.11 (11)	8.54 (35)	11.40 (09)
1000	250	38	8.66 (25)	12.92 (10)	0.00	11.19 (09)
		48	9.09 (22)	13.04 (10)	8.10 (35)	11.65 (09)
		67	9.65 (17)	12.97 (11)	8.38 (38)	10.83 (10)
	275	46	7.00 (38)	11.93 (11)	0.00	8.76 (24)
		66	0.00	11.38 (13)	0.00	9.49 (16)

tal data, because overly optimistic estimates of the magnitude of experimental uncertainties (for example, assigning the standard error of track measurements in a single run as the total experimental uncertainty) can lead to spurious preferences between models with negligibly different goodness-of-fit.

Variability of initial track lengths

The mean etchable length of confined fission tracks in geological samples is rarely observed to exceed 15 μm, significantly less than the mean etchable length of relatively unannealed, induced fission tracks, which generally exceeds 16 μm (e.g., Green 1980; Gleadow et al. 1986). This observation has been attributed to the residence of natural fission tracks at or near Earth surface temperatures for a million years or more. In their study of Cretaceous volcaniclastic apatites from Ocean Drilling Program drillhole 800A in the East Mariana Basin, Vrolijk et al. (1992) demonstrated the presence of significant etchable length reduction of natural fission tracks that likely did not experience temperatures in excess of 21 °C. Furthermore, experiments have confirmed that annealing of induced fission tracks occurs at ambient temperatures in the laboratory (Donelick et al. 1990).

Laslett et al. (1987) offered the first detailed use of initial fission-track length as a reference point for interpreting thermal histories from natural fission-track populations. Several authors have followed their lead and offered measurements of this type for calibration purposes (e.g., Crowley et al. 1991; Donelick 1991). More recently, Laslett and Galbraith (1996) presented a refinement to the approach of Laslett et al. (1987) in which they allowed initial mean fission-track length to be a free parameter in their efforts to derive fission-track annealing formulations for use in length modeling.

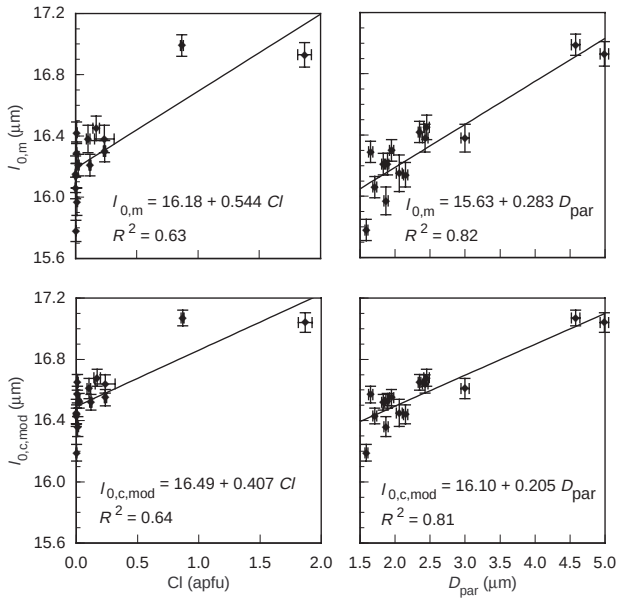

FIGURE 1. Variation of mean initial track lengths with Cl content of apatite and etch-pit diameter for all 15 apatites in our experimental data set. Etching conditions (20 s in 5.5 *M* HNO_3 at 21 °C) were uniform for all apatites. Upper diagrams plot measured initial track lengths; lower diagrams plot initial track lengths derived from experimental data by models presented in Ketcham et al. (1999, this volume).

Initial lengths measured for our unannealed apatites (Run 0 in Appendix Tables 2 and 3) show variations among apatites of different composition that are much greater than their individually calculated precisions. The total spread of mean lengths is ~1.2 μm; even among the near-end-member F-apatites, the spread is almost 0.7 μm. In standard annealing models (e.g., Laslett et al. 1987), a half-micrometer variation in initial track length leads to a difference of roughly 10–15 °C in predicted temperature along the later, cooler portions of a time-temperature path; if ascribed tectonic significance, such a difference can correspond to perhaps half a kilometer of unroofing.

Fortunately, the observed variation in initial lengths appears systematic with respect to some measurable parameters. In Figure 1 we present example functions that relate initial mean track length ($l_{0,m}$) and initial modeled *c*-axis projected track length ($l_{0,c,mod}$; cf. Ketcham et al. 1999, this volume) to etch-pit diameter (D_{par}) and chlorine content. Each of the fitted lines was calculated using a least-squares criterion that takes into account measurement errors for lengths, etch figures, and Cl determination. The equations for the fitted lines are:

$$l_{0,m} = 15.63 + 0.283\ D_{par}\ (\mu m);\ R^2 = 0.817 \quad (1)$$

$$l_{0,c,mod} = 16.10 + 0.205\ D_{par}\ (\mu m);\ R^2 = 0.814 \quad (2)$$

$$l_{0,m} = 16.18 + 0.544\ Cl\ (apfu);\ R^2 = 0.627 \quad (3)$$

$$l_{0,c,mod} = 16.49 + 0.407\ Cl\ (apfu);\ R^2 = 0.644 \quad (4)$$

The correlations of $l_{0,m}$ and $l_{0,c,mod}$ with D_{par} can be understood in terms of apatite bulk-etching characteristics. In past studies of apatite fission-track annealing, analysts have performed a simple etching experiment to determine optimal etching conditions for the apatites they investigated. A good example of this is provided by Crowley et al. (1991, their Fig. 1). Such experiments typically provide data on mean track length versus etching time while holding the etchant composition and temperature constant. We applied this procedure to apatite DR to produce the results compiled in Table 3 and plotted in Figure 2 along with Equation 1 for comparison. The DR data plotted in Figure 2 roughly parallel the line based on Equation 1 although, without exception, the data plot above it. Because the data for variable etching of this single apatite specimen (Fig. 2) correlate with etch-pit diameter, producing a linear trend in the data very similar to that produced by identical etching of multiple apatites (Fig. 1), we infer that apatite etching characteristics are the primary source of the variations in initial mean track lengths among the 15 apatite specimens studied. It is noteworthy that the DR data plotted in Figure 2 were measured for a population of induced fission tracks different from the population used to derive the above equations, the former having been irradiated for only the first 37 minutes of the 197 total minutes for the DR specimen listed in Table 1. As 9 of the 15 apatite specimens used to derive the above equations were irradiated for more than 100 minutes, the possibility exists that some amount of thermal annealing of the induced fission tracks occurred while the apatites were near the reactor core. This would account for the observation that the DR data plotted in Figure 2 lie above the plotted line.

The correlations of l_m and $l_{c,mod}$ with Cl can be understood in a similar fashion, because Cl content is grossly but imperfectly correlated with D_{par}. Variations in Cl content lead to variations in initial fission-track lengths to the extent that Cl correlates with D_{par}. This notion is supported by the better correlations exhibited by the lines based on D_{par} as opposed to Cl content.

Investigators who use the same etching conditions as those employed in this study can probably utilize the above relations if they renormalize them according to their own measurements of initial induced track lengths for Durango apatite. Investigators who use different etching conditions would be advised to compile their own data set of apatite etching characteristics and/or composition versus initial induced track length and to construct relations analogous to those presented above.

Variability of annealing rates

The experimental data in this study confirm and quantify substantial variations in the rate at which fission tracks in apatite anneal when heated. A graphic illustration of the magnitude and importance of this variability is provided by the comparison in Figure 3 among the measured extents of annealing in a single experimental run, and the considerably smaller differences among predictions made by various quantitative annealing models in the literature. Although much discussion has centered upon which model should be preferred for use in thermal history analysis, these data make it clear that model differences can be dwarfed by natural variability in annealing behavior, even when consideration is restricted to the range of compositions likely to be encountered commonly in natural settings.

Also significant is the nearly identical annealing behavior of the six apatite specimens with very similar compositions close to the $Ca_{10}(PO_4)_6F_2$ end-member (OL, UN, RN, WK, SC, and PQ). Their similar behavior suggests that chemical composition is the predominant cause of variation in annealing kinetics, although other possible factors (perhaps including variability in etching response, structural strain, or the extent of α-damage in the crystal) may also play a role. It should be remembered, however, that all specimens were heated to eradicate existing fission tracks prior to irradiation; thus the possible effects on annealing rates of natural structural defects and accumulated radiation damage in crystals may be masked in experimental studies.

Prediction of annealing rates from composition, structure, or etching rates

The factors producing large variations in annealing rates are evidently quite complex, and we have not yet been able to determine them from the data at hand. Our experimental annealing data cannot be accounted for entirely by either of the two single controls previously hypothesized, namely the Cl content of the apatite (cf. Green et al. 1986) and its total ionic porosity (Z) (cf. Carlson 1990). Using D_{par} to infer relative resistance to annealing (e.g., Burtner et al. 1994) similarly accounts for some, but not all, of the variability revealed by these experiments. For example, apatites with small values of D_{par} exhibit annealing behavior similar to that of the $Ca_{10}(PO_4)_6F_2$ end-member, but apatites with larger values of D_{par} span the entire range of annealing behaviors.

To study this problem, we use as our indicator of relative resistance to annealing among apatites the parameter r_{mr0} (defined in detail in Part III), which characterizes the annealing behavior of any chosen apatite in comparison with the most-resistant apatite in the data set. As used here, r_{mr0} is the estimated reduced length of the most-resistant apatite (B2) at the laboratory time and temperature conditions where that length in the less-resistant apatite being characterized falls to zero. Thus small values of r_{mr0} correspond to a high degree of resistance to annealing. As illustrated by the plots of r_{mr0} against Cl content, D_{par}, and total ionic porosity in Figure 4, the likely effects of these variables are apparently convoluted with other factors that disrupt any direct correlation between them and the degree of resistance to annealing displayed by any given apatite.

Additional compositional (and associated crystallographic) factors must be important determinants of annealing rates, and there is likely to be a complex interplay among several factors that separately accelerate and inhibit annealing. We have unsuccessfully sought correlations between resistance to annealing and various compositional parameters, including the total amount of substitution relative to a $Ca_{10}(PO_4)_6F_2$ end-member; the amount of separate substitution on the ^{VII}Ca and ^{IX}Ca sites, the P site, and the halogen site (assignments as shown in Table 4); and the amounts of various substituents singly and in combination.

It is possible, of course, to produce an empirical best fit of the annealing data to some functional combination of the compositional variables. For the sake of completeness, we include

TABLE 3. Mean track lengths for Durango apatite etched for different times in 5.5 *M* HNO_3 at 21 °C

Etch time (s)	D_{par} (μm)	No. of tracks measured	Mean angle to *c* axis (degrees)	l_m (μm)	l_c (μm)	l_a (μm)	σ_m (μm)	σ_e (μm)
15	1.43 (13)	111	60.95	16.16 (08)	16.52 (27)	16.03 (11)	0.81	0.81
20	1.91 (14)	122	62.57	16.32 (08)	17.00 (28)	16.11 (10)	0.83	0.81
30	2.34 (10)	112	57.72	16.42 (09)	16.75 (21)	16.27 (11)	0.92	0.91
40	3.11 (13)	112	58.46	16.94 (08)	17.21 (20)	16.82 (10)	0.80	0.80
50	3.85 (17)	112	55.15	17.05 (09)	17.75 (18)	16.68 (11)	0.93	0.88
60	4.98 (15)	113	56.39	17.45 (08)	17.61 (19)	17.37 (11)	0.82	0.82

Note: These DR slabs are from the same megacryst as the DR specimen used in the annealing experiments, but were irradiated for only the first 37 minutes of the total 197 minutes. Additionally, these DR slabs were irradiated with approximately 10^7 ^{252}Cf-derived fission tracks per cm^2 prior to etching to enhance the TINT fission track measurability. Numbers in parentheses are one standard error in least significant digit. Meaning of symbols: l_m = arithmetic mean track length; l_c = mean track length parallel to the *c* axis; l_a = mean track length perpendicular to the *c* axis; σ_m = standard deviation of track-length measurements; σ_e = the standard deviation of the distribution of track lengths about their best-fit ellipse, calculated via Equation 3 of Donelick (1991).

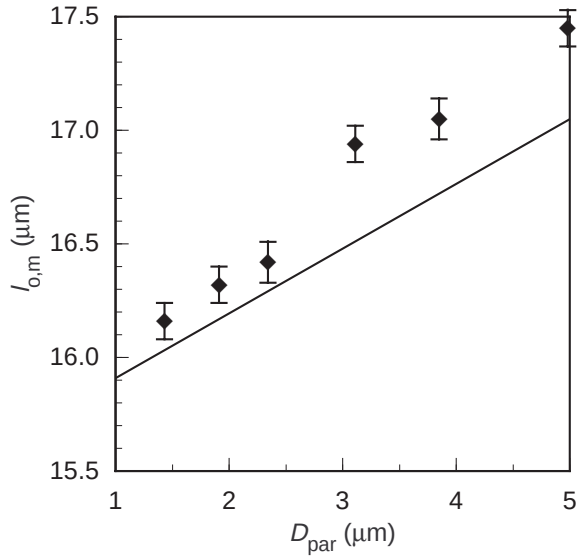

FIGURE 2. Correlation between measured initial track length and etch-pit diameter for Durango apatite etched for varying intervals (15–60 s) in 5.5 *M* HNO_3 at 21 °C. Line plots the relationship between these quantities fitted to the experimental data in Figure 1 for all apatites under uniform etching conditions. The fact that the Durango data fall above the fitted line for the 15-apatite set may be explained by differences in exposure time during neutron irradiation, as discussed in text.

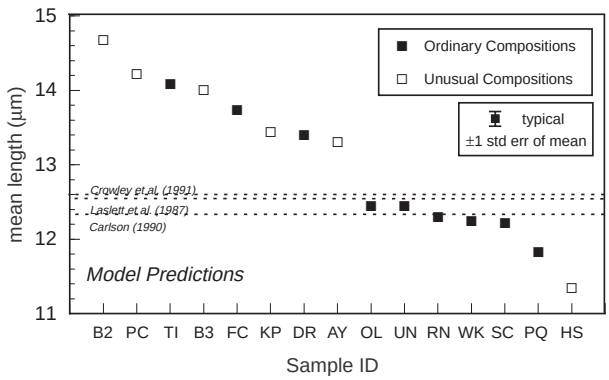

FIGURE 3. Data from a single annealing experiment, demonstrating the magnitude of variation in annealing rates among apatites of different composition. These differences in annealing behavior are nearly an order of magnitude greater than the discrepancies among the three recent mathematical annealing models fitted to prior experimental data on Durango apatite (values indicated by dashed lines), even when extreme compositional variants (open symbols) are not considered. Note that annealing models are based on data of Green et al. (1986) for Durango apatite; the systematic discrepancy between that data set and the present work is reflected in the departure of the models from the measured value for DR in this diagram. Five apatites close in composition to a $Ca_{10}(PO_4)_6F_2$ end-member (OL, UN, RN, WK, SC) all show degrees of annealing that are equivalent within measurement error; a sixth apatite of similar composition (PQ) is only slightly more annealed. These similarities suggest that compositional variation dominates over other possible factors as a cause of variability in annealing kinetics.

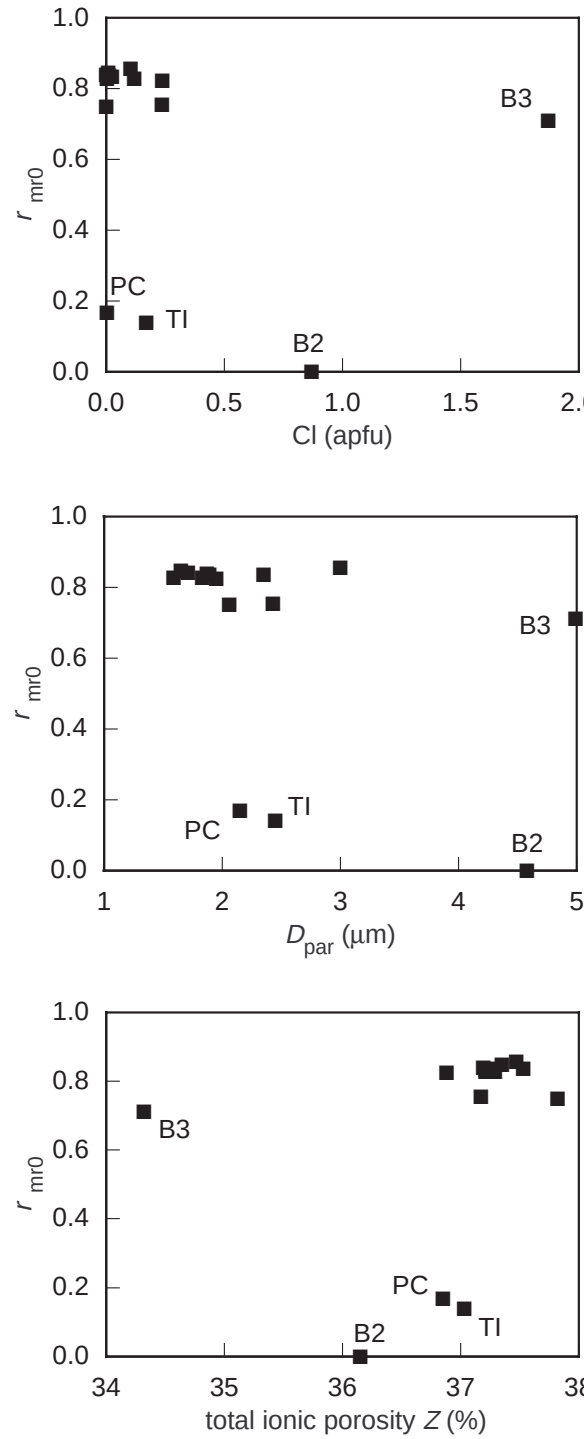

FIGURE 4. Data illustrating inability of Cl content, etch-pit size, and total ionic porosity to account for variations in annealing kinetics over the full range of compositions studied. Although each of these apatite characteristics appears to have limited predictive value over a restricted range of compositions, additional factors or interactions among possible factors (or both) must play significant roles in determining annealing rates.

TABLE 4. Substitutions (apfu) in 2835 detrital apatites

Site	Substituent	Percentiles										
		10	20	30	40	50	60	70	80	90	95	99
F	Cl	0.003	0.013	0.023	0.044	0.065	0.089	0.122	0.174	0.280	0.406	0.533
	OH	0.086	0.178	0.254	0.322	0.395	0.482	0.564	0.643	0.749	0.840	1.054
P	Si	0.000	0.000	0.020	0.029	0.036	0.044	0.050	0.059	0.080	0.105	0.203
	S	0.000	0.000	0.000	0.000	0.000	0.000	0.000	0.001	0.004	0.009	0.036
	U	0.000	0.000	0.000	0.000	0.000	0.000	0.000	0.000	0.000	0.001	0.002
	Th	0.000	0.000	0.000	0.000	0.000	0.000	0.000	0.000	0.002	0.003	0.006
^{IX}Ca	Na	0.000	0.000	0.003	0.010	0.013	0.017	0.023	0.030	0.044	0.063	0.103
	Mn	0.000	0.004	0.006	0.007	0.009	0.012	0.013	0.017	0.024	0.033	0.059
^{VII}Ca	Fe	0.000	0.000	0.006	0.012	0.019	0.028	0.039	0.052	0.066	0.076	0.096
	Sr	0.000	0.000	0.001	0.003	0.005	0.006	0.009	0.013	0.021	0.037	0.093
	Ba	0.000	0.000	0.000	0.000	0.000	0.000	0.000	0.000	0.001	0.003	0.007
	REE*	0.000	0.003	0.007	0.009	0.012	0.015	0.020	0.027	0.063	0.091	0.152

Note: Sites of predominant substitution for Na, Mn, Fe, Sr, and REE are based on determinations made by Hughes et al. (1991a), Hughes et al. (1991b), Hughes et al. (1993), and Fleet and Pan (1997); other sites of substitution are assumptions based only on similarities of ionic radii. Although REE are listed as substituents on the ^{VII}Ca site, they partition between ^{VII}Ca and ^{IX}Ca in roughly a 2:1 ratio (Hughes et al. 1991b; Fleet and Pan 1997). Similarly, Mn partitions strongly, but not exclusively, into ^{IX}Ca (Hughes et al. 1991a). REE* indicates total of all analyzed rare earth elements.

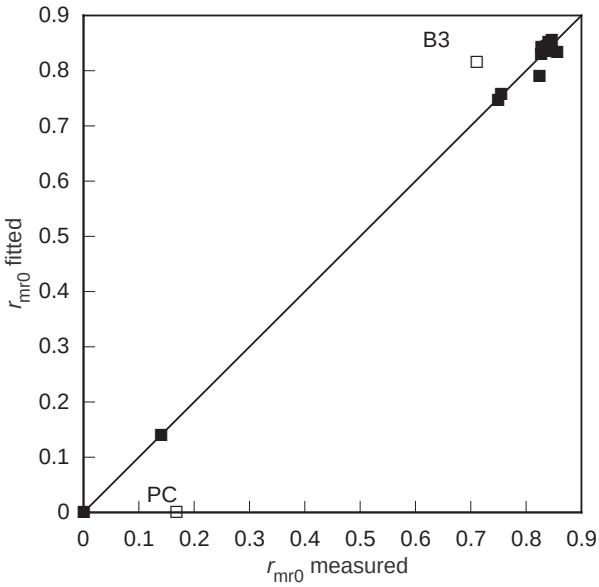

FIGURE 5. Annealing behavior predicted from apatite compositions, based on Equation 6 of text. Specimens shown with open symbols, representing extreme compositional variants, were excluded from the fit that produced the depicted correlation. Because so few specimens actually constrain this fit [at most five data points fall outside of the cluster dominated by near end-member $Ca_{10}(PO_4)_6F_2$ compositions], its predictive ability is suspect and caution in its application is urged.

such an analysis here. Although we stress that such an approach will not allow confident prediction of annealing behavior for apatites of arbitrary composition, it calls attention to the relative magnitudes of the potential effects of various compositional factors. We used an expression with the form

$$r_{mr0} = [a_0 + a_1x_1 + a_2x_2 + \cdots + a_nx_n]^{\alpha} \quad (5)$$

in which the purpose of the exponent is to compensate for the nonlinearity of the relationship between r_{mr0} and closure temperature (cf. Ketcham et al. 1999, this volume). We obtained the best fit by neglecting apatites B3 and PC, which have the most unusual compositions, resulting in the expression:

$$r_{mr0} = [0.027 + 0.431 \text{ abs (Cl} - 1) + 0.107 \text{ abs (OH} - 1) - 1.01 \text{ Mn} - 2.67 \text{ Fe} - 0.144 \text{ Others}]^{0.25}. \quad (6)$$

In this expression, compositional variables are in terms of apfu for a $Ca_{10}(PO_4)_6F_2$ end-member, and "Others" is the sum of all measured cations aside from Fe and Mn that substitute for calcium (Sr, Ce, La, and Na). The expressions for OH and Cl are cast in the way shown to reflect a rough apparent symmetry in which apatites with end-member compositions in these substituents are apparently less resistant to annealing than apatites with more mixing. This equation reproduces the observed annealing behavior in these experiments to the level of agreement shown in Figure 5. The relative magnitudes of the coefficients can be used together with the data in Table 4 to estimate the relative significance of each of these compositional variables. However, in the absence of any physical understanding of why compositional variations impede or enhance annealing, we have little confidence that it can be used meaningfully to predict the annealing behavior of apatites not included in the experiments. For example, the effect of Fe concentration is determined entirely by the annealing behavior of a single extremely Fe-rich apatite. Nonetheless, these data appear to suggest that substituents for Ca tend to reduce rates of annealing, and that annealing kinetics depend upon the degree of mixing on the halogen site, in some still-concealed and probably complex way.

Although several extreme compositional variants were included in these experiments in the hope of gaining greater physical understanding, many applications of apatite fission-track annealing to thermal-history determinations will be concerned with only the subset of data that approximates the range of compositions commonly encountered in sedimentary rocks. A sense of the range of commonly encountered compositions is provided by a set of 2835 analyses of apatite made by Donelick Analytical, Inc., in the course of commercial fission-track projects. Table 4 lists the frequency with which various levels of substituents occur; for example, the table shows that 80% of the analyzed apatites incorporated Cl at levels below 0.174 apfu, based on the end-member formula $Ca_{10}(PO_4)_6F_2$.

Comparisons to experimental data from other sources

Because the present results include annealing data for apatite compositions identical or very similar to those used in prior

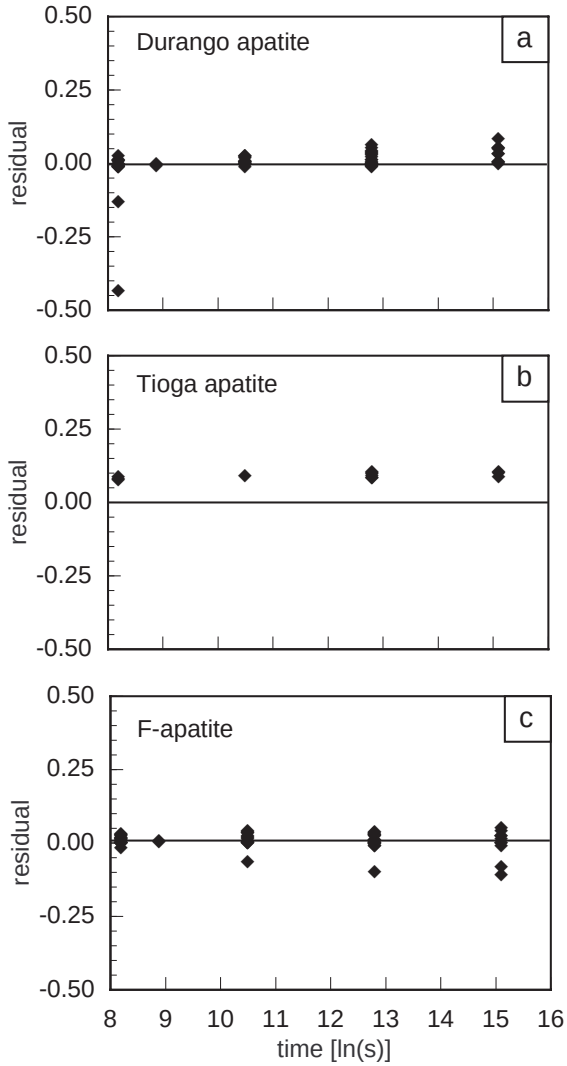

FIGURE 6. Interlaboratory comparison of experimental data on annealing kinetics. Because run times and temperatures are not identical in the experimental data sets, this diagram compares our experimentally determined reduced lengths to the reduced lengths predicted by best-fit models to prior experimental data sets; the residuals shown are the differences between the two. Data on the Durango apatite become increasingly discrepant at longer run times; data on the Tioga apatite are systematically discrepant; and data on the near end-member Ca-F apatite are uniformly in good agreement. As discussed in the text, these discrepancies probably are ascribed best to differences in the thermal control and measurement protocols: better agreement exists between data sets for which greater care in temperature control and measurement was documented.

annealing studies, interlaboratory comparisons are now possible. Prior experimental work that can be compared to the present results includes the pioneering studies on Durango apatite by Green et al. (1986) and Duddy et al. (1988); the study of the Tioga apatite by Donelick (1988); and the study of near-end-member $Ca_{10}(PO_4)_6F_2$ apatite (specimen B-5) by Crowley et al. (1991). We find that systematic differences exist between our new data and some of these prior studies, which may be attributable to experimental procedures, particularly the control and measurement of annealing temperatures.

Figure 6 affords a comparison between our present data and those of Green et al. (1986, Fig. 6a), Donelick (1988, Fig. 6b), and Crowley et al. (1991, Fig. 6c). Because run times and temperatures were different in each of these studies, the comparison is made by plotting the difference between the reduced length measured in our experiments and the reduced length calculated from best-fit models to the experimental data of others. The experiments of Green et al. (1986) on Durango apatite correspond well to our experiments at short run times (with two exceptions), but display systematically shorter mean track lengths for long run times. The experiments of Donelick (1988) on Tioga apatite produced systematically shorter mean track lengths for all run times. The experiments of Crowley et al. (1991) on a near-end-member Ca-F apatite (B-5) are in generally good agreement with our experiments on a similar composition (RN) over the full range of experimental run times.

Interlaboratory agreement appears to be better for those data sets for which greater effort was expended to achieve accurate and precise temperature control. Our present results do not agree well with those of Donelick (1988). The experiments of Donelick (1988) were performed with apparatus similar in design to that used in this study, but temperature calibrations were not as rigorous. The comparison in Figure 6b suggests that the actual annealing temperatures achieved in the study of Donelick (1988) are systematically high by ~20–25 °C relative to our present results. Adjusting the temperatures cited by Donelick (1988) downward by this amount would bring that data set into generally good agreement with our own measurements on the Tioga apatite.

Better, but incomplete, agreement exists between our results and those of Green et al. (1986), who report on the precision but not the accuracy of their experimental temperatures. Those experiments were carried out in a vertical tube furnace "controlled to ±3 °C in early work, and ±1 °C in later studies …using a thermocouple inserted into the furnace in the vicinity of the samples" (Green et al. 1986, p. 239). The best agreement exists between our results and those of Crowley et al. (1991), who describe (p. 1450) care taken to eliminate thermal gradients and fluctuations, cross-calibration of thermocouples to establish measurement precision, and an estimate of accuracy of ±2 °C (although the basis for this estimate is unstated).

Because interlaboratory comparisons are best in those cases for which the greatest effort was apparently expended to achieve accurate and consistent run temperatures, we believe that differences in thermal control, calibration, and measurement are the most likely explanations for discrepancies among the data sets from different sources.

CONCLUSIONS

This study provides quantitative confirmation that natural compositional variation in apatites is sufficient to produce marked differences in the resistance to annealing of apatite fission tracks. Unfortunately, useful correlations have yet to be determined between resistance to annealing and various compositionally dependent quantities (e.g., Cl content, total ionic porosity, etch-pit size); none of these factors can account com-

pletely for annealing behavior over the full range of compositions studied. Empirical fits suggest that annealing rates may be slower in specimens with appreciable substitution for Ca by other cations, and may depend in a complex way on the extent of mixing on the halogen site. Interlaboratory comparison of experimental annealing data reveals systematic differences that are probably best explained by contrasts in thermal control, calibration, and measurement.

Although rates of annealing vary widely, embedded in these experimental data are orderly relationships that permit a complete yet simple description of relative rates of annealing across the full range of composition. These relationships form the basis of a comprehensive empirical multikinetic annealing model presented in Ketcham et al. (1999, this volume).

ACKNOWLEDGMENTS

This research was supported by Grant 28367-AC2 from the American Chemical Society—Petroleum Research Fund to W.D.C., and by Donelick Analytical, Inc. The Geology Foundation of the University of Texas at Austin helped to defray costs of publication. We are grateful to the following individuals and institutions for providing apatite samples: Casey Ravenhurst; Sorena Sorenson and the National Museum of National History; Mark Cloos; Bob Gaits and the Royal Ontario Museum; Don Miller; Mary Roden-Tice; and Peter Wallace. James Rougvie assisted with the powder XRD work and the determination of cell parameters. Stefan Boettcher and Fangqiong Lu performed the electron microprobe analyses of the experimental apatites. We thank Steve Bergman and ARCO Research (Plano) for providing independent microprobe analyses for comparison. Helpful reviews were provided by Kerry Gallagher, Mark Brandon, and Robert Dymek.

REFERENCES CITED

Albee, A.L. and Ray, L. (1970) Correction factors for electron probe microanalysis of silicates, oxides, carbonates, phosphates, and sulfates. Analytical Chemistry, 42, 1408–1414.

Burtner, R.L., Nigrini, A., and Donelick, R.A. (1994) Thermochronology of lower Cretaceous source rocks in the Idaho-Wyoming Thrust Belt. American Association of Petroleum Geologists Bulletin, 78, 1613–1636.

Carlson, W. (1990) Mechanisms and kinetics of apatite fission-track annealing. American Mineralogist, 75, 1120–1139.

Crowley, K.D., Cameron, M., and Schaefer, R.L. (1991) Experimental studies of annealing of etched fission tracks in fluorapatite. Geochimica et Cosmochimica Acta, 55, 1449–1465.

Donelick, R.A. (1988) Etchable fission track length reduction in apatite: Experimental observations, theory and geological applications, Ph.D. dissertation, Rensselaer Polytechic Institute, New Jersey.

——(1991) Crystallographic orientation dependence of mean etchable fission track length in apatite: An empirical model and experimental observations. American Mineralogist, 76, 83–91.

——(1993) A method of fission track analysis utilizing bulk chemical etching of apatite. Patent No. 5,267,274, U.S.A.

——(1995) A method of fission track analysis utilizing bulk chemical etching of apatite. Patent No. 658,800, Australia.

Donelick, R.A., Roden, M.K., Mooers, J.D., Carpenter, S.B., and Miller, D.S. (1990) Etchable length reduction of induced fission tracks in apatite at room temperature (~23 °C): Crystallographic orientation effects and "initial" mean lengths. Nuclear Tracks and Radiation Measurements, 17, 261–265.

Duddy, I.R., Green, P.F., and Laslett, G.M. (1988) Thermal annealing of fission tracks in apatite 3. Variable temperature behaviour. Chemical Geology (Isotope Geoscience Section), 73, 25–38.

Fleet, M.E. and Pan, Y. (1997) Site preference of rare earth elements in fluorapatite: Binary (LREE+HREE)-substituted crystals. American Mineralogist, 82, 870–877.

Gleadow, A.J.W., Duddy, I.R., Green, P.F., and Lovering, J.F. (1986) Confined track lengths in apatite –A diagnostic tool for thermal history analysis. Contributions to Mineralogy and Petrology, 94, 405–415.

Green, P.F. (1980) On the cause of the shortening of spontaneous fission tracks in certain minerals. Nuclear Tracks and Radiation Measurements, 4, 91–100.

Green, P.F., Duddy, I.R., Gleadow, A.J.W., Tingate, P.R., and Laslett, G.M. (1986) Thermal annealing of fission tracks in apatite 1. A qualitative description. Chemical Geology (Isotope Geoscience Section), 59, 237–253.

Honess, A.P. (1927) The nature, origin, and interpretation of the etch figures on crystals. 171 p. Wiley, New York.

Hounslow, A.W. and Chao, G.Y. (1970) Monoclinic chlorapatite from Ontario. Canadian Mineralogist, 10, 252–259.

Hughes, J.M., Cameron, M., and Crowley, K.D. (1989) Structural variations in natural F, OH, and Cl apatites. American Mineralogist, 74, 870–876.

——(1991a) Ordering of divalent cations in the apatite structure: Crystal structure refinements of natural Mn- and Sr-bearing apatite. American Mineralogist, 76, 1857–1862.

Hughes, J.M., Cameron, M., and Mariano, A.N. (1991b) Rare-earth-element ordering and structural variations in natural rare-earth-bearing apatites. American Mineralogist, 76, 1165—1173.

Hughes, J.M., Fransolet, A.-M., and Schreyer, W. (1993) The atomic arrangement of iron-bearing apatite. Neues Jahrbuch für Mineralogie, Monatshefte, 11, 504–510.

Laslett, G.M. and Galbraith, R.M. (1996) Statistical modelling of thermal annealing of fission tracks in apatite. Geochimica et Cosmochimica Acta, 60, 5117–5131.

Laslett, G.M., Green, P.F., Duddy, I.R., and Gleadow, A.J.W. (1987) Thermal annealing of fission tracks in apatite 2. A quantitative analysis. Chemical Geology (Isotope Geoscience Section), 65, 1–13.

Novak, G.A. and Colville, A.A. (1989) A practical interactive least-squares cell-parameter program using an electronic spreadsheet and a personal computer. American Mineralogist, 74, 488–490.

Stormer, J.C. Jr., Pierson, M.L., and Tacker, R.C. (1993) Variation of F and Cl X-ray intensity due to anisotropic diffusion in apatite during electron microprobe analysis. American Mineralogist, 78, 641–648.

Vrolijk, P., Donelick, R.A., Queng, J., and Cloos, M. (1992) Testing models of fission track annealing in apatite in a simple thermal setting: Site 800, Leg 129. Proceedings of the Ocean Drilling Program, Scientific Results, 129, 169–176.

MANUSCRIPT RECEIVED JUNE 8, 1998
MANUSCRIPT ACCEPTED MAY 3,1999
PAPER HANDLED BY ROBERT F. DYMEK